Xe adsorption on a C_{60} monolayer on Ag(111)

S. M. Gatica,[1,*] H. I. Li,[2] R. A. Trasca,[3] M. W. Cole,[2] and R. D. Diehl[2]
[1]*Department of Physics and Astronomy, Howard University, 2355 Sixth Street, NW, Washington, DC 20059, USA*
[2]*Department of Physics, Pennsylvania State University, University Park, Pennsylvania 16802-5000, USA*
[3]*Institut für Theoretische Chemie, C7, TU Berlin, 10623 Berlin, Germany*
(Received 4 September 2007; published 18 January 2008)

Low-energy electron diffraction (LEED) experiments and grand canonical Monte Carlo simulations were carried out to study the adsorption of Xe on a substrate composed of a monolayer of C_{60} molecules on a Ag(111) surface. LEED adsorption isobars indicated that the adsorption occurs in steps, with the Xe initially adopting a structure having the same unit cell as the C_{60}. Isosteric heats corresponding to the first two steps were measured to be 234 ± 8 and 204 ± 14 meV, respectively. For the simulations, the interaction potential of Xe with the composite substrate was modeled as the sum of two parts: the Xe-Ag part was computed using an *ab initio* van der Waals potential that varies as an inverse-distance cubed and the Xe-C_{60} part was computed using a spherically averaged C_{60} potential [E. S. Hernandez *et al.*, J. Low Temp. Phys. **134**, 309 (2004)]. The resulting adsorption potential is highly corrugated, with the most attractive sites located in the threefold hollows between the C_{60} molecules, forming a honeycomb array. The simulations (at temperatures ranging from 55 to 90 K) show that these attractive sites are filled first, followed by adsorption in two types of secondary sites, where a competition exists due to steric hindrance. The thermodynamic properties of film growth obtained in the simulation are in good agreement with the experiment.

DOI: 10.1103/PhysRevB.77.045414 PACS number(s): 68.43.−h, 61.05.jh, 68.43.Fg, 61.48.−c

I. INTRODUCTION

The adsorption of gases in nanostructures is relevant to many potential applications to nanotechnology. For example, fullerenes are currently being explored for applications such as gas sensors and gas storage. Because of their relative simplicity, they also provide an ideal opportunity to extend our fundamental knowledge of the interaction of gases with nanostructures. A persistent question in such applications is the role of epitaxy in film growth. A film on C_{60} provides an intermediate step between the well-studied case of adsorption on atomically flat substrates[2,3] and adsorption on complex porous materials.[4–6]

The central question to be addressed in this paper concerns the phase evolution and growth of adsorbed Xe, as the pressure (P) and temperature (T) are varied. On flat substrates, for example, graphite, Xe forms a two-dimensional (2D) gas at very low coverage, followed by the creation of incommensurate 2D islands. During the growth of these islands, there is a characteristic step in the isotherm or isobar, which ends in the completion of the monolayer, the structure of which is essentially that expected for 2D Xe. Similar isotherm (isobar) steps are observed during the formation of the second and subsequent layers.[2,3] On nanostructured substrates, the morphology of the substrate plays a larger role in the film growth. For example, on a bundle of carbon nanotubes, adsorption starts in the grooves between pairs of neighboring tubes, forming an array of lines of atoms, instead of a flat 2D monolayer.[4–6] The effect of the nanostructure relief is usually much reduced in the second and successive layers, however.

Because of the difficulty of carrying out structural measurements for adsorbates on such complex substrates, little is known about the effect of what essentially amounts to a strongly nanocorrugated (as opposed to atomically corrugated) substrate on the atomistic properties of such films. The present study addresses this lack by studying the adsorption of Xe on a well-characterized substrate consisting of a monolayer of C_{60} molecules on Ag(111). The study combines low-energy electron diffraction (LEED) experiments on Xe adsorption on a C_{60} film with grand canonical Monte Carlo (GCMC) simulations of the same system in order to elucidate the effect of the highly corrugated, nanostructured substrate on the adsorption properties of Xe.

The outline of this paper is the following. In Sec. II, we describe the LEED experiments for Xe adsorption on a substrate composed of a C_{60} monolayer on Ag(111). In Sec. III, we describe the calculation of the Xe-substrate potential for the same system and the results of the GCMC simulations. In Sec. IV, we discuss our findings.

II. LOW-ENERGY ELECTRON DIFFRACTION EXPERIMENT

A. Procedure

The Ag(111) crystal was cut from a single crystal Ag rod using a wire saw, oriented with Laue x-ray diffraction and polished to within 0.15° of the {111} plane. The surface was polished with a diamond polishing compound having successively finer grit size, finishing with 0.25 μm grit, and then chemically etched. The chemical etch was a solution of saturated chromic acid diluted 10:1 with water, adding two drops of HCl to 15 ml of the final solution. This solution was applied to the crystal surface with a polishing pad for a few seconds, after which the surface was rinsed with water and dried with acetone. The crystal was prepared in the ultrahigh vacuum chamber by repeated cycles of 30–60 min of Ar ion bombardment (0.5 keV) followed by annealing to 500 °C. After several cycles, the Ag(111) LEED pattern displayed

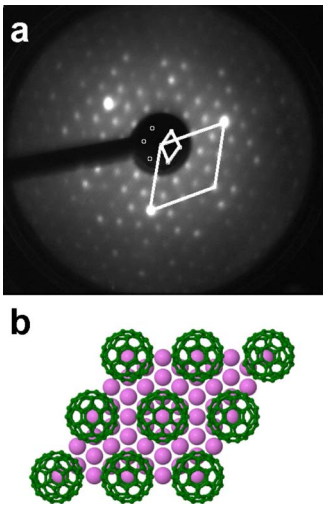

FIG. 1. (Color online) (a) LEED pattern from the C_{60} monolayer on Ag(111) at $T=32$ K for an incident beam energy of 300 eV. The unit cells (in reciprocal space) for Ag(111) (large rhombus) and the $(2\sqrt{3}\times 2\sqrt{3})R30°$ structure (small rhombus) are indicated. (b) Schematic structure model for the C_{60} monolayer (Ref. 19.)

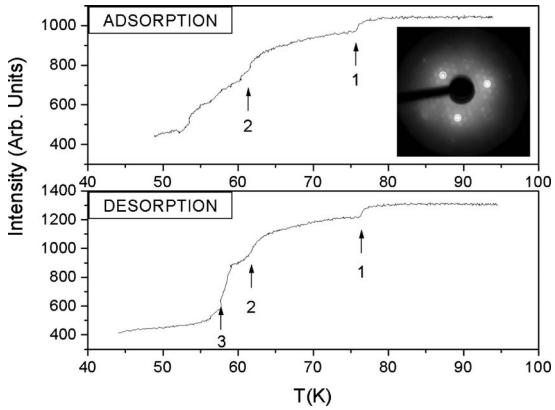

FIG. 2. LEED intensity isobars for Xe (a) adsorption and (b) desorption at 1.7×10^{-7} mbar on the C_{60} monolayer on Ag(111). These intensities are the averaged integrated intensities of the three bright first-order Ag(111) diffraction spots (indicated by circles on the inset LEED pattern).

sharp spots with low background intensity, and there were no detectable impurities in the Auger spectrum.

The C_{60} monolayer was grown by subliming C_{60} from a source that consisted of 99.95+% pure C_{60} powder inside an open Pyrex tube that was wrapped with a Ta heater wire. The T of the C_{60} during dosing, measured using a type-K thermocouple sealed into the Pyrex tube and in contact with the C_{60} powder, was 260 °C. At this T, it took about 45 min to grow a C_{60} film several layers thick. The T of the Ag(111) during dosing was around 50 °C. After dosing, the sample was heated to 415 °C for a few minutes to desorb the multilayers, leaving a well-ordered commensurate $(2\sqrt{3}\times 2\sqrt{3})R30°$ monolayer of C_{60}.[7] The LEED pattern for this structure at 32 K is shown in Fig. 1(a). The structure of this monolayer has been determined by a LEED intensity analysis to consist of C_{60} molecules adsorbed with hexagonal faces down, as shown in Fig. 1(b).[8] This structure forms the substrate for the Xe adsorption studies described here.

Xe adsorption isobars were measured by holding the Xe pressure constant while raising or lowering the temperature of the substrate. The temperature scans were taken at an average rate of about 5 K/min, using a slower rate at the low T's and a higher rate at the higher T's. The LEED data collection consisted of recording the LEED pattern at a primary beam energy of 391 eV using a charge-coupled device camera interfaced to a personal computer via Data Translation frame grabber and processor boards. This beam energy was chosen to maximize the intensity of the first-order Ag(111) diffraction spots, thus providing a greater dynamic range for the measurements of intensity attenuation as Xe is adsorbed. The integrated intensities of the diffraction spots were obtained by integrating the pixels inside a circular window centered on the diffraction spot and subtracting a planar background fit to the pixels on the window perimeter.

The Xe pressure was measured using a nude ion gauge. The gauge reading was corrected for the Xe calibration factor, and it was further corrected for the difference in the T of the gas at the surface and the impinging room-temperature gas using the thermomolecular correction,

$$P_{surface} = P_{gauge}\left(\frac{T_{surface}}{T_{gauge}}\right). \quad (1)$$

B. Results

LEED intensity isobars were measured for several different pressures for both heating and cooling. Two such spectra are shown in Fig. 2 for $P=1.7\times 10^{-7}$ mbar. These spectra have been corrected for the Debye-Waller factor of the substrate by fitting the natural logarithm of the intensity of the high-T section of the data (before Xe adsorbs) and dividing the entire spectrum by the resulting slope.

Two steps are clearly evident during the adsorption (decreasing T) curves, whereas three clear steps are seen in the desorption (increasing T) curves. An apparent third step near $T=53$ K is due to pressure fluctuations that sometimes occur during the low-T part of the cooling procedure, where the cooling rate is very slow. The highest-T step occurs at about 76 K in both cases, and there is very little hysteresis in this step. The next step occurs at about 63 K in both cases. A distinct third step can be seen in the desorption curve at about 58 K, but the adsorption curve shows a more gradual intensity change between about 53 and 60 K. The same qualitative difference (more discontinous desorption than adsorption) is a common feature of hysteretic adsorption behavior and is seen commonly in porous media and in nanostructured systems.[9,10]

The diffraction spots that were measured have intensity contributions from the scattering from both the Ag(111) and the C_{60} structures, although the Ag(111) contribution is attenuated by the C_{60}. When the Xe adsorbs, there are no new diffraction features observed, but the intensity of all diffraction features decreases. The simplest interpretation is that the Xe forms a disordered film, but we believe that this is in-

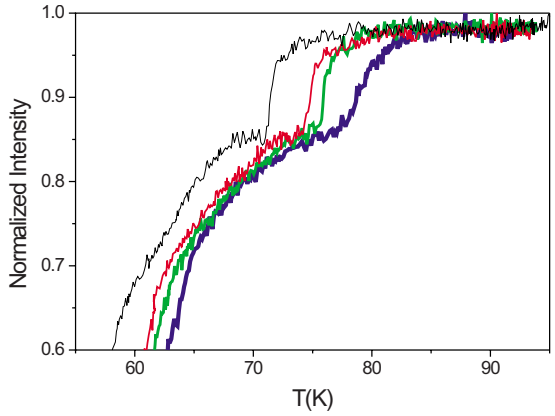

FIG. 3. (Color online) Family of adsorption isobars showing the intensity of the substrate diffraction spot (shown in Fig. 2) as a function of T for (from right to left) 5.2×10^{-7}, 1.7×10^{-7}, 8.5×10^{-8}, and 1.4×10^{-8} mbar.

compatible with the steps observed in the isobars, for reasons that will become clear later. Therefore, the most likely interpretation is that the Xe initially forms a structure having the same unit cell, implying that the Xe also contributes diffraction intensity to the spots we are measuring, at the same time as attenuating the scattering from the Ag and C_{60}. Because of this complex combination of diffraction and attenuation effects, the use of the intensities to quantify how much Xe is adsorbed for each step of the isobars is not possible. This deficiency is addressed with the Monte Carlo simulations described below.

The stepwise adsorption and desorption of the Xe on this surface imply that there are specific sites having distinct binding energies and that distinct layers form. The isosteric heat of adsorption q_{st} corresponding to each step can be determined by measuring a family of isobars, as shown in Fig. 3, to obtain the P and T dependence of the isobar steps. The P and T locations of the first two isobar steps are shown in Fig. 4 on a ln P vs $1/T$ graph. The isosteric heats are derived from the slopes of these curves using

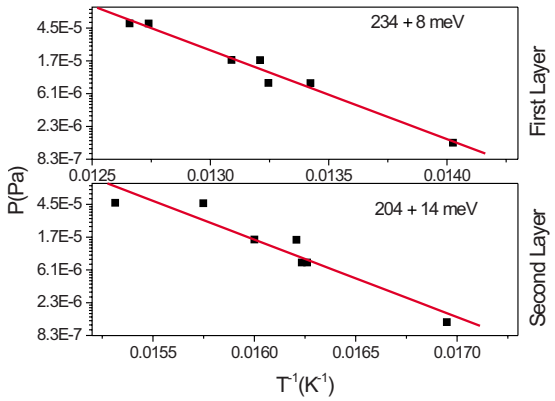

FIG. 4. (Color online) Locations in P and T of the first and second isobar steps, respectively. The y axis is on a natural logarithmic scale (P in Pa$\approx10^{-2}$ mbar). The isosteric heats derived from the slopes of the lines are indicated.

$$q_{st} = -k_B \left.\frac{d\ln P}{d(1/T)}\right|_N, \tag{2}$$

where the derivative is done at constant coverage.

The average values thus obtained are 234 ± 8 and 204 ± 14 meV for the first and second steps, respectively. Based on the Monte Carlo simulations described below, we interpret these steps to correspond to adsorption in the threefold hollows between C_{60} molecules (first step) and to adsorption in a mixture of bridge sites between C_{60} molecules (second step). The third step in the isobars, which are well defined only in the desorption spectra, occurs very close to the bulk vapor pressure values for Xe.[11]

III. MONTE CARLO SIMULATIONS

A. Method of calculation

The substrate was modeled using the experimentally derived Ag(111)-2($\sqrt{3}\times2\sqrt{3}$)$R30°$ structure shown in Fig. 1(b).[8] The distance from the Ag(111) surface to the closest hexagon of the C_{60} is 2.31 Å and the center-to-center distance between C_{60} molecules is 10.01 Å. The interaction between a Xe atom and the substrate has two contributions, from the Ag(111) and from the C_{60}; the latter contribution dominates due to the balls' proximity to the adlayer.

The Xe-Ag(111) interaction was modeled in the continuum approximation by the rigorous asymptotic form of the van der Waals interaction (including many-body corrections), $V_{Ag}(d)$. This results in

$$V_{Ag}(d) = -\frac{C}{d^3}, \tag{3}$$

where d is the distance to the image plane edge of the Ag surface and C is the van der Waals coefficient, set equal to 2.34 eV Å^3.[12] The interaction of the Xe with the C_{60} molecules was calculated as a sum of contributions $V_{C_{60}}(r)$ from each C_{60} molecule in the simulation cell and first-neighboring cells. For $V_{C_{60}}$, we used an analytical, spherically symmetric form,[1] calculated by integrating the C-Xe interaction over a spherical shell of continuum carbon with an areal density $n=0.38$ Å^{-2},

$$V_{C_{60}}(r) = 4\pi nR\varepsilon_{gs}\frac{1}{r}\left\{\frac{\sigma_{gs}^{12}}{5}\left[\frac{1}{(r-R)^{10}}-\frac{1}{(r+R)^{10}}\right] - \frac{\sigma_{gs}^{6}}{2}\left[\frac{1}{(r-R)^{4}}-\frac{1}{(r+R)^{4}}\right]\right\}. \tag{4}$$

Here, $R=3.55$ Å, $\varepsilon_{gs}=78.7$ K, and $\sigma_{gs}=3.75$ Å, and r is the distance to the center of the molecule. This approximation ignores the atomicity of the C_{60} molecules. The resulting potential $V_{C_{60}}$ (from a single C_{60}) has a minimum value of -790 K (-68.1 meV) at $r_{min}=7.3$ Å. This value is about 40% of the well depth for a Xe atom on flat graphite.[12] For the Xe-Xe interaction, we use the well-known Lennard-Jones (LJ) potential

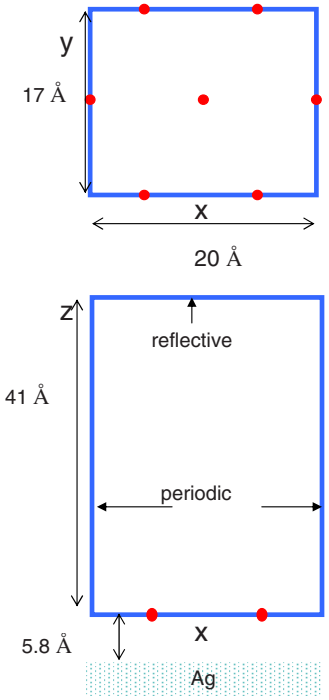

FIG. 5. (Color online) Diagram of the simulation cell, not to scale. The red dots represent the positions of the centers of the C_{60} molecules.

$$V_{LJ}(r) = 4\varepsilon\left[\left(\frac{\sigma}{r}\right)^{12} - \left(\frac{\sigma}{r}\right)^{6}\right], \tag{5}$$

where the LJ parameters are $\varepsilon = 221$ K and $\sigma = 4.1$ Å, and r is the Xe-Xe separation.[13]

Figure 5 shows the simulation cell. The base is a 20×17.3 Å^2 rectangle located in the plane that contains the centers of the C_{60} molecules. There is one C_{60} molecule at the center of the cell and six molecules on the perimeter. The height of the cell is 41 Å ($10\sigma_{\text{Xe-Xe}}$). The boundary conditions are periodic in the x and y directions and reflective in the z direction at the top of the cell.

The energetics of rare gas films on an array of C_{60} molecules was investigated previously for the case of $T=0$, finding that the total substrate potential exhibits a pattern of very attractive sites.[14] The most attractive of these sites are located in the threefold hollows between C_{60} molecules at a distance $r_{\text{min}} = 5.83$ Å away from each other. Those "hollow sites" (H) are depicted in Fig. 6. Two other secondary minima lie above the line that joins two C_{60} molecules; these we call the "bridge" (B) and "center bridge" (C) sites (see Fig. 6). The sites H, B, and C are located 4.4, 7, and 5.2 Å, respectively, above the plane that contains the center of the C_{60}'s.

Figure 7 shows the substrate potential following a surface-normal line above each site as a function of the distance to the base of the cell. The contribution of the Ag(111) at the position of the H sites is only −12 K, about 200 times smaller than the minimum of $V_{C_{60}}$. We have computed the adsorption behavior of Xe on this substrate by GCMC simulations. We refer the reader to an earlier work[15] for details of the simulation method. Here, a total of 4×10^6 moves were computed for each value of P and T. The first 3×10^6 moves were discarded during equilibration, and from the last 10^6, 10^4 moves were used to perform the averages of the observables.

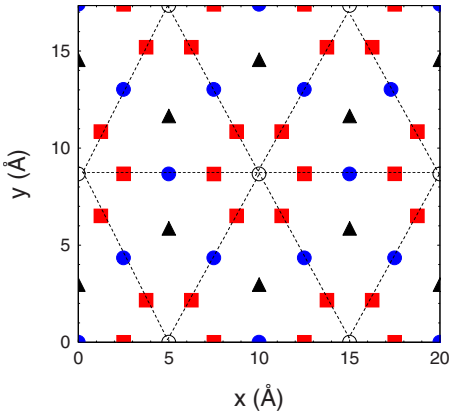

FIG. 6. (Color online) Schematic view of the positions of sites H (black triangles), B (red squares), and C (blue circles) projected on the simulation cell. The empty circles represent the centers of the C_{60} molecules. Each set of sites is contained on three planes parallel to the base of the cell at different heights.

B. Results

We computed the equilibrium values of the energy, coverage per unit area N, and density $\rho(\mathbf{r})$ at T values between 55 and 90 K for a wide range of P. Figure 8 shows isotherms N vs P for $T=60$, 65, 77, and 90 K. In all curves, we observe two clear steps, and a third step only visible at the lower temperatures. The first step, a sudden jump from $N=0$ to 0.023 Å^{-2}, corresponds to the occupation of the most attractive H sites.

In Fig. 9(a), we display the 2D average density, $n_2(x,y)$, defined as the integral of the three-dimensional (3D) atomic density $\rho(\mathbf{r})$ over the surface-normal (z) direction

$$n_2(x,y) = \int \rho(r)dz \tag{6}$$

for $N=0.023$ Å^{-2} and $T=60$ K. We see in this figure that the Xe atoms are found only at H sites. The coverage of this

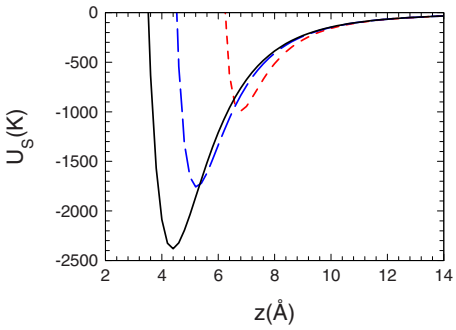

FIG. 7. (Color online) Adsorption potential as a function of distance above the sites H (solid black line), B (dashed red line), and C (long-dashed blue line).

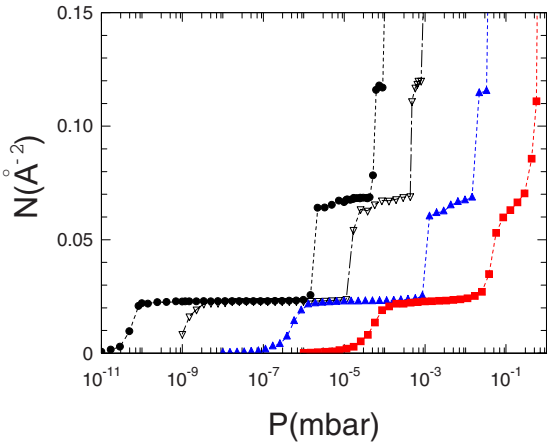

FIG. 8. (Color online) Adsorption isotherms for $T=60$, 65, 77, and 90 K (from left to right). The dotted lines are guides to the eyes.

phase (phase H) remains stable for a wide range of P. For example, at $T=60$ K, the phase H exists from $P=10^{-10}$ to 10^{-6} mbar.

At higher P, we find a second step in the isotherm that corresponds to the abrupt occupation (near $N=0.065$ Å^{-2}) of sites B and C, forming a layer of Xe atoms above those in the H sites. The coverage thereafter increases slowly with P. The 2D density at the end of this step is shown in Fig. 9(b). Here, we see high-density areas around sites H, B, and C. Note that only half of the B sites are occupied. This is because the Xe atoms are too large to fill all six B sites around each C_{60}, causing them to take alternating sites instead.

We also observe that C sites, which might seem more attractive than the B sites, as shown in Fig. 7, are not filled

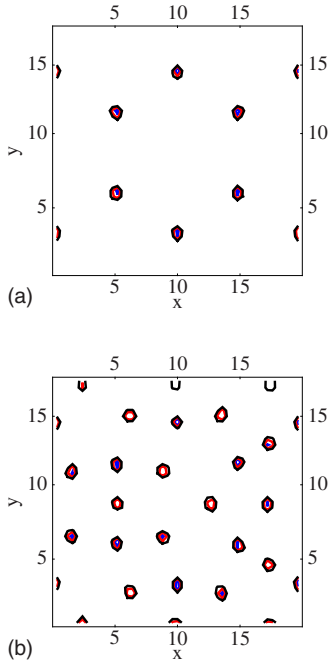

FIG. 9. (Color online) Contour plots of the 2D density $n_2(x,y)$ for phases (a) H and (b) BC. Contours correspond to $N=0.5$ Å^{-2} (black, outer), 1 Å^{-2} (red, middle), and 2 Å^{-2} (blue, inner).

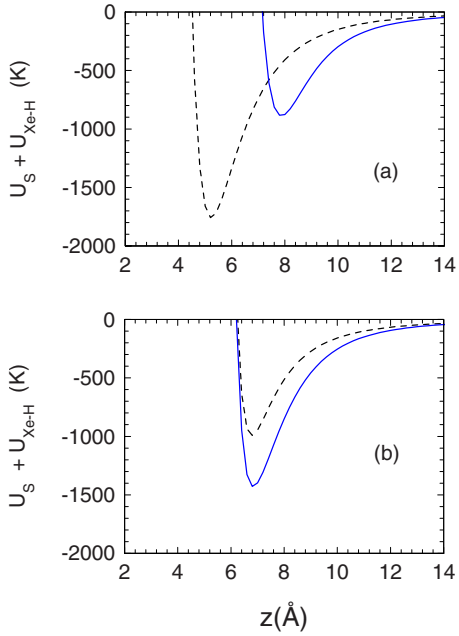

FIG. 10. (Color online) Effective potentials due to both the substrate with Xe atoms at the H sites at the locations of (a) the C sites and (b) the B sites (solid-blue line). The bare substrate (unfilled H sites) potential is also shown (dashed line) for comparison.

until after the B sites. Disregarding the size of the Xe atoms, one might expect the C sites to be filled before the B sites. However, when the H sites are already full, they create a steric repulsion extending to the C sites. In Fig. 10, we show the effective potential due to the substrate and the filled H sites. As one can see, the inclusion of the filled H site interactions enhances the attraction at B sites, while C sites are less attractive. In fact, the C sites that are occupied in Fig. 9(b) are not at the originally calculated height (Fig. 6) but are located at $z=8$ Å.

A third discontinuous increase in the coverage manifests the formation of a third layer. This phase extends over a small range of P and is followed by a multilayered film. For higher T, the scenario is similar, but the steps are more rounded due to thermal effects. In order to study the location of the layers along the z axis, we calculate the relative coverage defined as

$$\nu(z) = \nu_{mono}^{-1} \int \rho(r) dx dy, \tag{7}$$

where $\nu_{\text{mono}}=0.0613$ Å^{-2} is the number of Xe atoms per unit area found in 2D solid Xe. In Fig. 11, we show $\nu(z)$ at $T=60$ K and at the pressures 1.4×10^{-6}, 2.4×10^{-5}, and 5.88×10^{-5} mbar, corresponding to phases H, BC, and the third layer, respectively. The coverage of phase H is equivalent to 37% of a Xe monolayer and the Xe atoms are distributed within a narrow range in z of about 0.5 Å. Phase BC's position is 2.6 Å above the atoms in the H sites and extends over a z range of approximately 2 Å. These atoms contribute 73% of a monolayer, making the total coverage of 1.1 ML (monolayer) at this P. In the third step, the atoms populate a third

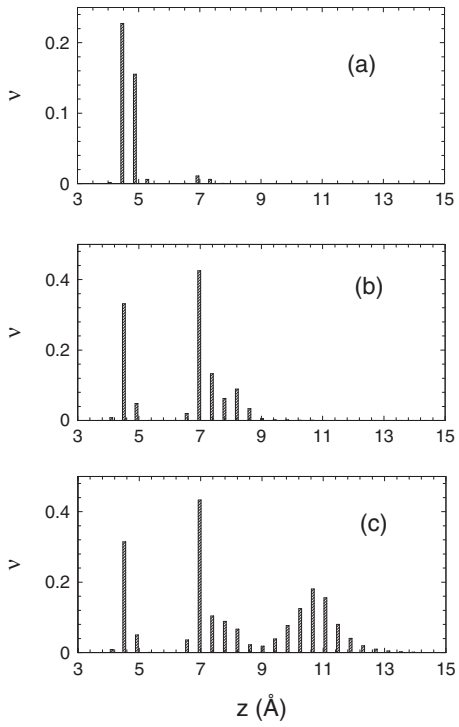

FIG. 11. Relative coverage as a function of z for $T=60$ K and $P=$(a) 1.4×10^{-6} mbar, (b) 2.4×10^{-5} mbar, and (c) 5.8×10^{-5} mbar.

layer that is approximately 4 Å above the atoms in the B sites and is distributed over a z range of about 4 Å. Its partial coverage is about 0.8 ML, giving total coverage at this P that is equivalent to almost 2 ML. Increasing P further produces a film with additional layers separated by about 4 Å, as shown in Fig. 12 for $T=60$ K and $P=7.2\times10^{-4}$ mbar. Table I contains additional values of P at which each phase occurs, for several T's, information that is complementary to Fig. 8.

We next evaluate the isosteric heat of adsorption, as in the experiments, by computing the slope of the curve $\ln P$ vs $1/T$. We do this calculation for two values of the coverage,

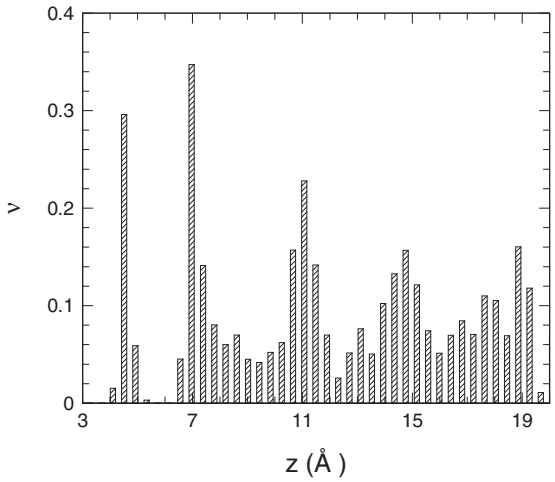

FIG. 12. Relative coverage as a function of z for $T=60$ K and 7.2×10^{-4} mbar.

TABLE I. Pressures, in mbar, at which the transitions to the phases H and BC, third layer, and bulk film occur at each temperature.

T (K)	H	BC	Third layer	Film
55	2.2×10^{-12}	1.9×10^{-7}	1.1×10^{-5}	2.5×10^{-5}
60	8.0×10^{-11}	2.2×10^{-6}	6.0×10^{-5}	1.0×10^{-4}
65	3.0×10^{-9}	1.7×10^{-5}	6.5×10^{-4}	1.5×10^{-3}
70	3.4×10^{-8}	1.1×10^{-4}	2.9×10^{-3}	6.6×10^{-3}
74	3.8×10^{-7}	8.5×10^{-4}	9.7×10^{-3}	3.3×10^{-2}
77	1.3×10^{-6}	1.3×10^{-3}	2.2×10^{-2}	7.4×10^{-2}
83	8.6×10^{-6}	8.5×10^{-3}	9.7×10^{-2}	2.2×10^{-1}
86	2.6×10^{-5}	1.7×10^{-2}	1.9×10^{-1}	4.3×10^{-1}
90	1.0×10^{-4}	5.0×10^{-2}	[a]	6.0×10^{-1}

[a]This step is not observed.

$N=0.01$ Å^{-2} and $N=0.05$ Å^{-2}. These represent the values of N for which the H and B sites, respectively, are half-filled. The result of the calculation is displayed in Fig. 13, where a linear fit was computed. We obtained $q_{st}=213$ meV for the H sites and $q_{st}=153$ meV for the B sites. The former value is 5.3% smaller and the latter value is 15% smaller than the experimental results described above.

Figure 14 shows a comparison of an adsorption isobar derived from the simulation data to the experimental isobar for $P=1.7\times10^{-7}$ mbar. The key features in the latter are steps at 76 and 63 K, which show no hysteresis, as shown in Fig. 2. The corresponding steps in the calculated isobar occur

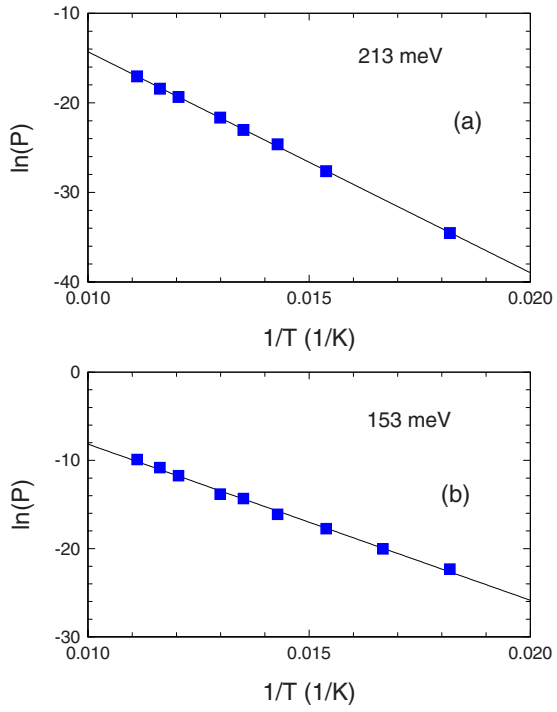

FIG. 13. (Color online) $\ln P$ vs $1/T$ for (a) $N=0.01$ Å^{-2} and (b) $N=0.05$ Å^{-2}. The lines are the linear fits and the isosteric heats derived from the slopes are given on the graphs.

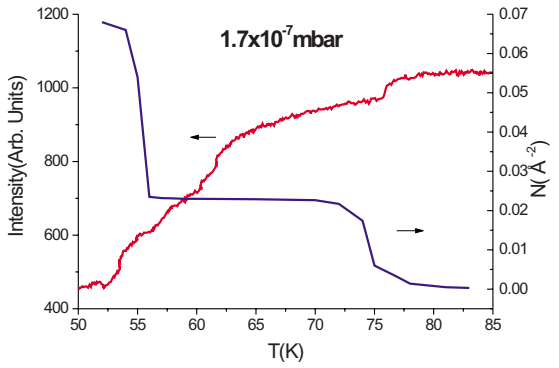

FIG. 14. (Color online) Experimental (red, left axis) and simulated (blue, right axis) adsorption isobars at $P=1.7\times10^{-7}$ mbar.

at approximately 74 and 55 K. These two steps arise from adsorption at sites *H* and *BC*, respectively.

IV. DISCUSSION AND CONCLUSIONS

The principal points of comparison between the experimental and simulation results are (1) the step-by-step adsorption behavior observed in the isobars or isotherms, (2) the *T*, *P* locations of the steps, and (3) the heats of adsorption derived from the isobars. The same step structure was observed in both the experiment and the simulations, and the good correspondence allows us to use the simulations to interpret the experimental results. It also provides a measure of the validity of the assumptions used in the calculations.

We have found that the steps in the isobars (isotherms) correspond to adsorption in specific sites on the C_{60} film. The first step corresponds to adsorption in the strong-binding *H* sites, which are the threefold hollows between C_{60} molecules. We note that a similar preference for these sites has been observed for Au clusters adsorbed on a C_{60} monolayer.[16] When these sites are occupied (two Xe atoms per unit cell), the unit cell of the Xe structure is the same as that of the substrate, and therefore no superstructure spots should be produced in diffraction, as observed. The second step corresponds to adsorption in the *B* and *C* sites, which are located on the bridges that join C_{60} molecules. Although the *C* sites (see Fig. 6) are stronger binding sites for Xe on the bare C_{60} film, the *B* sites become more favorable when the *H* sites are occupied, due to steric factors. The second step results from adsorption in both *B* and *C* sites, with the *B* sites being occupied (3 Xe atoms per unit cell) slightly before the *C* sites (1 Xe atom per unit cell).

The heats of adsorption corresponding to the first step were found to be 234 ± 8 and 213 meV from the experiment and simulations, respectively. We note first that the experimental heat of adsorption is essentially the same as that found for Xe adsorption on flat graphite [239 meV (Ref. 3)]. This was slightly unexpected since a Xe atom in a hollow between C_{60} molecules has a higher adatom-substrate coordination than Xe on flat graphite. However, the heat of adsorption includes a contribution from the Xe-Xe interactions, which are strongly attractive (~-70 meV per atom) on flat graphite but essentially nonexistent (<0.5 K) in the hollow sites of C_{60} because they are so far apart. This lateral interaction contributes about 25% to the heat of adsorption on flat graphite,[17] which suggests that the substrate contribution to q_{st} for these hollow sites is about 25% greater than for flat graphite.

Although the q_{st} values for the first step are statistically consistent, there is a larger deviation between the corresponding values for the second step, which are 204 ± 14 and 153 meV for experiment and simulations, respectively. In addition, the simulation value for the second step is smaller than the latent heat of sublimation for bulk Xe [161 meV (Ref. 11)]. It is not unexpected, then, that the steps in the isobars from the simulations occur at somewhat lower *T*'s than from experiment (Fig. 14), with a larger deviation found for the second step. Since we would expect that in the limit of bulk adsorption the measured heat of adsorption should correspond to the bulk heat of sublimation,[11] we also calculated the value for the highest accessible coverage in the simulation, $N=0.15$ A^{-2}, producing 132 meV. All of these results are consistent with a slight inaccuracy in the Xe-Xe potential and, indeed, such a discrepancy has been noted before for this potential.[18]

In spite of this slight discrepancy, the qualitative characteristics of the adsorption appear to be well described in the simulations presented here. There is also reasonable quantitative agreement for the adsorption of the first Xe atoms in the threefold hollows of the C_{60} molecules, which suggests that the Xe-C_{60} interaction potential is valid. This potential is based on quite simple, but plausible, assumptions. The most drastic assumption is the use of a pairwise additive Xe-C potential, ignoring the atomic structure of C_{60}. Such an assumption has produced reasonable consistency with experimental data for the case of gas adsorption on carbon nanotubes.[5] In that case, however, the Xe atoms are not commensurate with the underlying carbon structure, whereas in this case, they are. This approximation could be one of the reasons of having found a lower isosteric heat in the simulations compared to the experiment.

ACKNOWLEDGMENTS

We thank Stefano Curtarolo for useful advice concerning the simulations. This material is based on the work supported by the National Science Foundation under Grant No. 0505160. This research used resources of the National Energy Research Scientific Computing Center, which is supported by the Office of Science of the U.S. Department of Energy under Contract No. DE-AC02-05CH11231.

*Corresponding author. sgatica@howard.edu

[1] E. S. Hernandez, M. W. Cole, and M. Boninsegni, J. Low Temp. Phys. **134**, 309 (2004).
[2] L. W. Bruch, M. W. Cole, and E. Zaremba, *Physical Adsorption: Forces and Phenomena* (Dover, Mineola, NY, 2007).
[3] L. W. Bruch, R. D. Diehl, and J. A. Venables, Rev. Mod. Phys. **79**, 1381 (2007).
[4] M. M. Calbi, M. W. Cole, S. M. Gatica, M. J. Bojan, and G. Stan, Rev. Mod. Phys. **73**, 857 (2001).
[5] M. M. Calbi, M. W. Cole, S. M. Gatica, M. J. Bojan, and J. K. Johnson, in *Adsorption by Carbons*, edited by E. J. Bottani and J. M. D. Tascón (Elsevier, Amsterdam, 2008), pp. 187–210.
[6] A. D. Migone, in *Adsorption by Carbons* (Ref. 5), pp. 403–430.
[7] S. T. Shipman, S. Garrett-Roe, P. Szymanski, A. Yang, M. L. Strader, and C. B. Harris, J. Phys. Chem. B **110**, 10002 (2006).
[8] H. I. Li, K. H. Hanna, R. D. Diehl and W. Moritz, Bull. Am. Phys. Soc. 52, paper X19–5; http://meetings.aps.org/link/BAPS.2007.MAR.X19.5
[9] E. Kierlik, P. A. Monson, M. L. Rosinberg, L. Sarkisov, and G. Tarjus, Phys. Rev. Lett. **87**, 055701 (2001).
[10] M. M. Calbi, S. M. Gatica, M. J. Bojan, and M. W. Cole, J. Chem. Phys. **115**, 9975 (2001).
[11] J. Unguris, L. W. Bruch, E. R. Moog, and M. B. Webb, Surf. Sci. **87**, 415 (1979).
[12] G. Vidali, G. Ihm, H.-Y. Kim, and M. W. Cole, Surf. Sci. Rep. **12**, 135 (1991).
[13] R. S. Berry, S. A. Rice, and J. Ross, *Physical Chemistry* (Oxford University Press, Oxford, 2000), Table 21.13.
[14] R. A. Trasca, J. Krim, and T. Coffey (unpublished).
[15] S. M. Gatica, M. J. Bojan, G. Stan, and M. W. Cole, J. Chem. Phys. **114**, 3765 (2001).
[16] H. Liu and P. Reinke, Surf. Sci. **601**, 3149 (2007).
[17] L. W. Bruch, Surf. Sci. **125**, 194 (1983).
[18] W. Setyawan, N. Ferralis, R. D. Diehl, M. W. Cole, and S. Curtarolo, Phys. Rev. B **74**, 125425 (2006).
[19] JMOL, an open-source JAVA viewer for chemical structures in three dimensions (http://www.mol.org).